ACS APPLIED MATERIALS & INTERFACES

Research Article

www.acsami.org

Surface-Engineered Growth of $AgIn_5S_8$ Crystals

Chia-Hung Lai,[‡] Ching-Yeh Chiang,[‡] Po-Chang Lin,[‡] Kai-Yu Yang,[†] Chi Chung Hua,[‡] and Tai-Chou Lee*[,†]

[†]Department of Chemical and Materials Engineering, National Central University, 300 Jhongda Road, Jhongli, Taoyuan 320, Taiwan

[‡]Department of Chemical Engineering, National Chung Cheng University, 168 University Road, Min-Hsiung, Chia-Yi 621, Taiwan

ABSTRACT: The growth of semiconductor crystals and thin films plays an essential role in industry and academic research. Considering the environmental damage caused by energy consumption during their fabrication, a simpler and cheaper method is desired. In fact, preparing semiconductor materials at lower temperatures using solution chemistry has potential in this research field. We found that solution chemistry, the physical and chemical properties of the substrate surface, and the phase diagram of the multicomponent compound semiconductor have a decisive influence on the crystal structure of the material. In this study, we used self-assembled monolayers (SAMs) to modify the silicon/glass substrate surface and effectively control the density of the functional groups and surface energy of the substrates. We first employed various solutions to grow octadecyltrichlorosilane (OTS), 3-mercaptopropyltrimethoxysilane (MPS), and mixed OTS−MPS SAMs. The surface energy can be adjusted between 24.9 and 50.8 erg/cm^2. Using metal sulfide precursors in appropriate concentrations, $AgIn_5S_8$ crystals can be grown on the modified substrates without any post-thermal treatment. We can easily adjust the nucleation in order to vary the density of $AgIn_5S_8$ crystals. Our current process can achieve $AgIn_5S_8$ crystals of a maximum of 1 μm in diameter and a minimum crystal density of approximately 0.038/μm^2. One proof-of-concept experiment demonstrated that the material prepared from this low temperature process showed positive photocatalytic activity. This method for growing crystals can be applied to the green fabrication of optoelectronic materials.

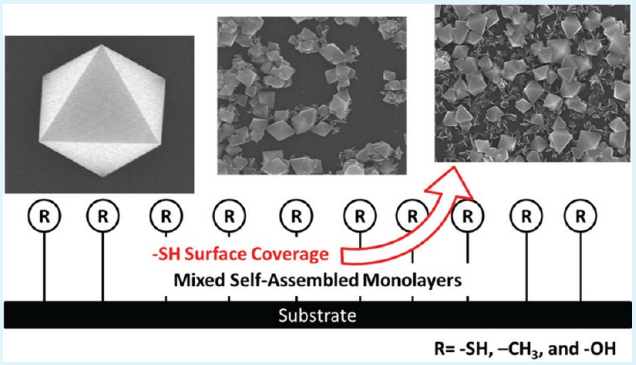

KEYWORDS: *self-assembled monolayers, surface modification, surface energy, low-temperature process, semiconductor, and crystal growth*

INTRODUCTION

Global warming and an efficient energy supply are among the most urgent issues. Ensuring a stable energy supply is crucial for national development. Currently fossil fuels are the primary sources of energy. Regardless of the number of years existing fossil fuels can sustain human activity,[1] the development of alternative energy must be accelerated to maintain sustainable human development. Take Taiwan for example, according to the energy supply status published by the Bureau of Energy, Ministry of Economic Affairs, and the Renewable Energy Development Bill passed by the Legislative Yuan in 2009, the target for renewable energy has increased from 6% in 2007 to approximately 15% by 2025.[2] Additionally, 96% of the energy in Taiwan is imported; thus, significant investment in renewable energy sources can increase the independence of Taiwan's energy supply and reduce pollutant emissions, providing multiple benefits through one action. In recent years, the effective use of solar energy has become a key research project in numerous countries. Nevertheless, whether it converts solar energy directly into electricity (photovoltaic), thermal energy (solar water heater), or chemical energy (biomass and hydrogen energy), a mediator is required to absorb solar energy and efficiently convert it into another form of energy for storage. The energy gap of semiconductors of the I−III−VI family is between 0.8 and 2.0 eV, which is considered an ideal light absorption layer.[3] They can be used not only in photovoltaic devices[4,5] but also as photoelectrodes in photochemical reactors.[6−10]

The thin films of the I−III−VI compound semiconductors can be fabricated by vacuum or solution chemistry. The former includes coevaporation,[5] Ag−In alloys or the sulfurization of Cu−In alloys,[11] reactive sputtering,[12] and chemical vapor deposition.[13] The latter includes spray pyrolysis,[14] electrodeposition,[15] photochemical deposition,[16] and chemical bath deposition (CBD).[17] To achieve the long-term goals of green chemistry, that is, to reduce the consumption of energy and material, the fabrication process should generate high-quality thin films and not be harmful to the environment.[18] Control of the solution chemistry by CBD and the interface between the solution and the substrate interface to generate thin films at

Received: July 23, 2012
Accepted: April 3, 2013
Published: April 3, 2013

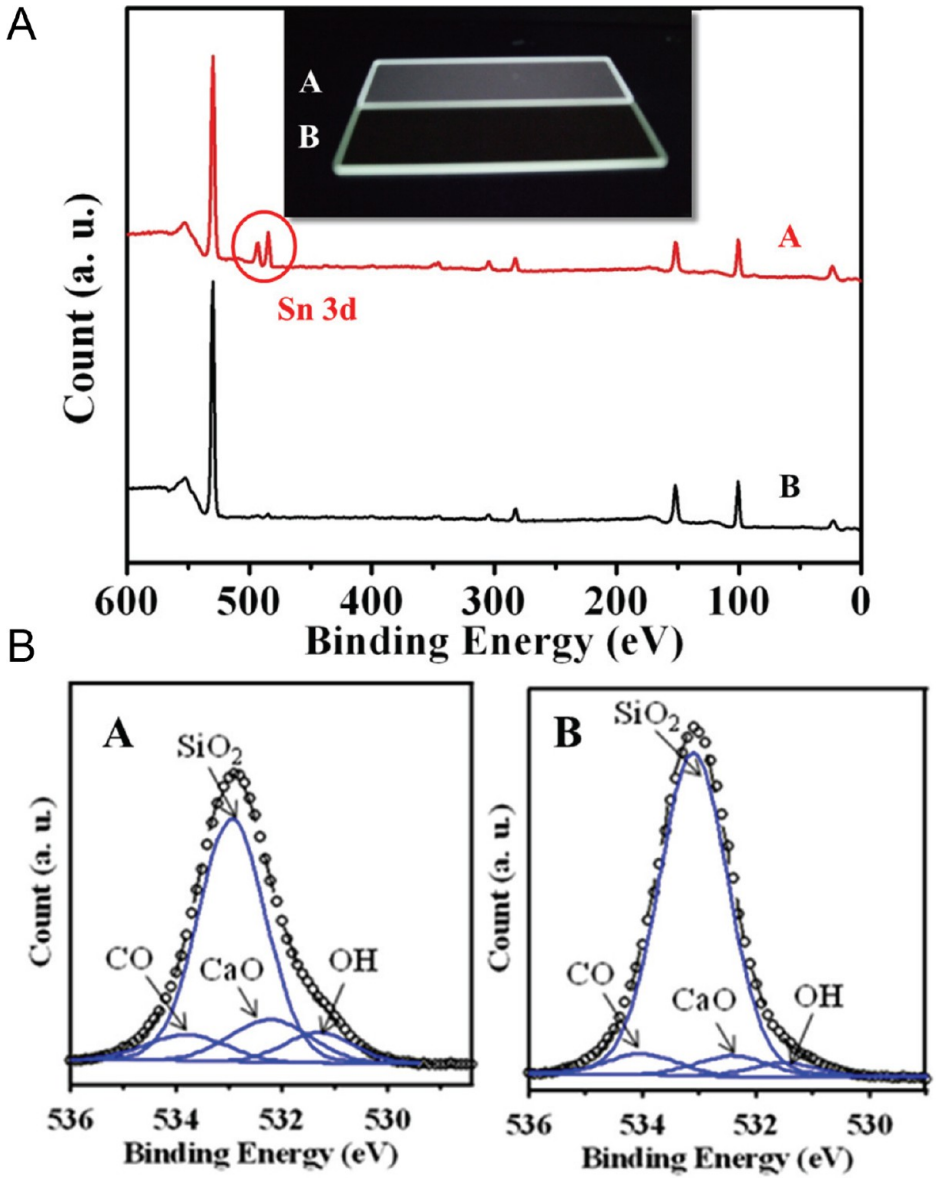

Figure 1. (a) XPS survey: (A) tin side; (B) air side of the glass substrate. (inset) Side A of the glass generates white fluorescent light under a UV lamp. (b) XPS O_{1s} high-resolution analysis: (A) tin side; (B) air side.

lower temperatures can satisfy these requirements. Thus, it provides a simple and cheap film-coating method. CBD is typically used to prepare binary metal sulfides. Sulfide ions are released slowly into the solution, react with the metal complex, and are then deposited on the substrate surface. Comprehensive studies have examined the film formation mechanism and coating criteria.[19−22] However, few reports have investigated the deposition of ternary oxide or sulfide compounds using CBD.[17,23−28] Because of the greater complexity of a solution system, the reaction mechanism is influenced by many ingredients: concentrations, pH values, chelating agents, temperature, etc. In addition to the solution chemistry mentioned above, an appropriate substrate surface is also a key parameter that determines the uniformity of a thin film.

Self-assembled monolayers (SAMs) are among the common methods used to modify the substrate surfaces. Effective control can be achieved by changing the chemical structure of a headgroup, tail group, chain length, and main chain structure. Thus, the surface properties of metal and semiconductor substrates, such as the wettability, biocompatibility, and corrosion resistance[29] can be cordially tuned. However, the greatest advantage of a SAM is that it forms a dense thin film on various types of substrate surfaces and alters the surface properties selectively and appropriately to meet the requirements. Changes of the surface functional group alter the interfacial tension between the solution and the substrate, resulting in influencing the nucleation mechanism. Therefore, an optimal system that effectively controls the property of substrate surfaces can be used to explore the impact of the tension between the solution and substrate on the growth of thin films. Metal sulfides can selectively deposit on SAMs.[30,31] These studies on growing mechanisms includes TiO_2 thin films grown on various SAM surfaces and changing coating processes such as changing the pH values for different solutions.[32] The binary compound semiconductor, such as CaP thin films can also be grown on a SAM substrate.[33,34] These studies indicate that combining SAM and chemical bath deposition methods has gradually received attention.

In this study, a simple solution process was used to generate Ag−In−S crystals for energy applications, typically hydrogen production from water splitting. One should keep in mind that the energy required to produce the materials or systems should not exceed the energy generated from the materials or systems. The advantages of using self-assembled monolayers are their flexibility and simplicity to modify the functionalities of the substrate surfaces. On the basis of our experience, properties of thin films deposited using chemical bath deposition depend strongly on the deposition process, i.e. nucleation and growth pathways. Both the solution chemistry and surface properties of the substrates have great influence on the deposition process. We have reported that an −SH terminated SAM can promote the nucleation of Ag_2S during the chemical bath deposition process.[25,26] In this study, we further investigated the physical original of $AgIn_5S_8$ crystal growth on the $-CH_3$ terminated SAM. By simply changing the ratio of OTS and MPS mixed SAMs, $AgIn_5S_8$ crystals can also be grown on these modified substrates without any further heat treatment. This provides a way to reduce the cost and energy during materials processing. As mentioned above, SAMs grown on a silicon wafer is a well-defined model system. This enables us to rule out other possible effects originated from the substrates. We thoroughly investigated the fundamental properties of SAMs on Si wafer and glass substrates first and then studied the growth mechanism and the impact of nucleation on the $AgIn_5S_8$ crystals. The same strategy can be applied to other systems, such as ITO substrates for photoelectrochemical applications.

EXPERIMENTAL SECTION

Materials. The chemicals required for the experiment, such as 3-mercaptopropyl-trimethoxysilane (MPS, >98%, Fluka), octadecyltrichlorosilane (OTS, >90%, Aldrich), anhydrous iso-octane (99.8%, Aldrich), toluene (>99.5%, J.T. Baker), chloroform (>99.8%, J. T. Baker), dichloromethane (>99.9%, J. T. Baker), silver nitrate (99%, J. T. Baker), indium(III) nitrate hydrate (99.99%, Aldrich), thioacetamide (99%, Fluka), triethanolamide (TEA, 99%, Riedel-de Haen), anhydrous citric acid (>99%, Sigma), sodium citrate tribasic dihydrate (>99%, Fluka), and ammonium nitrate (>98%, Riedel-de Haen), were purchased without further purification. For this study, we used P-type silicon wafers (1 0 0) and microscope glass slides as substrates. On the basis of the literature, the silicon wafer for the deposition of ultrasmooth OTS self-assembled monolayers (OTS-SAM) were cleaned using the following steps.[35] First, the substrates were sonicated in acetone and DI-H_2O for 5 min in an ultrasonic bath. Next, the substrates were soaked in an RCA (Radio Corporation of America) solution (RCA bath 1 (50:1:1 DI water:concentrated NH_4OH:30% H_2O_2) and bath 2 (50:1:1 DI water:concentrated HCl:30% H_2O_2) at 70 °C for 15 min each and then soaked in diluted HF solution (DI-H_2O:HF = 10:1) for 30 s to remove native SiO_2. Finally, the substrates were soaked in piranha (H_2SO_4:DI-H_2O = 7:3) solution for 30 min to generate the −OH functional group on the substrates. During each cleansing step, the substrates were thoroughly rinsed by DI-H_2O and dried in an oven at 125 °C. The glass slides were irradiated with UV light to identify the two sides.[36] The side of the glass that generated white fluorescent light under a UV lamp was considered side A (tin side); glass poured on the molten tin during the glass manufacture process (Figure 1a). Side B did not change its color under UV light. This is the air-side, and only pure silicon dioxide was presented (Figure 1a). The XPS survey analysis showed that side A of the glass had a significant Sn 3d characteristic peak, with binding energy between 480 and 500 eV (Figure 1a, curve A). Additionally, we used the high-resolution XPS to analyze the O 1s signals. Assuming that the O 1s characteristic peak has the same sampling area, the percentage of −OH on sides A and B are approximately 9% and 4%, respectively, as shown in Figure 1b. The roughness of these substrates differs. After the acid-washing procedure using piranha solution, the roughness measured by AFM was <1 nm for the silicon wafer, 2.38 nm for side A of the glass, and 1.25 nm for side B of the glass.

Self-Assembled Monolayers. We prepared two types of SAM, namely, MPS and OTS, and a mixture of these two SAMs. In our experiments, silicon wafers and glass substrates were used. The surfaces must first be cleaned by piranha to avoid contaminations by impurities and ensure that the −OH hydrophilic surface allows the monolayer to bond onto the glass surface. Because the organic solvent molecules have a significant influence on the quality of the generated monolayer, the selection of solutions is a key factor that controls the reaction. In a glovebox, the cleaned substrates are soaked separately in the prepared OTS solution, at a fixed concentration of 1 mM. After reacting for 4 h, the substrates are retrieved and soaked separately in toluene and acetone with sonication for 10 min. Subsequently, the substrates are removed, washed with deionized water, and dried using nitrogen. This experiment involved the following four types of solvents: anhydrous iso-octane, toluene, chloroform, and dichloromethane. The reaction temperature was maintained between 18 and 28 °C. To prepare the mixed SAMs, because OTS and MPS have different reactivities due to the difference in chain length and the surface-active headgroup, we adopted a two-step film formation method to control the density of functional groups on the surface. In the first step, we soaked the substrate in an MPS solution. Toluene was used as the solvent. The solution concentrations were 0.05, 0.1, 5, and 10 mM, respectively. The solution was left to settle for 30 min and then set aside. Next, we placed the MPS-modified silicon substrates in an OTS solution with dissolved in anhydrous iso-octane at various concentrations (0.05 mM/0.1 mM/5 mM/10 mM) to form an MPS−OTS mixed SAM. After settling for 4 h, the substrates were cleaned using an iso-octane solution and dried by nitrogen. Next, we reversed the soaking sequence for comparison. The substrates were soaked in OTS for 30 min during the first step and in MPS for 4 h during the second step to investigate the surface property changes. The preparation of mixed SAMs was carried out at 28 °C.

Chemical Bath Deposition of $AgIn_5S_8$ on SAM-Modified Surfaces. Semiconductor thin films grown in solution can be prepared using simple equipment. Specifically, only precursors, breakers, and a heating element with magnetic stirrer are required. To prepare I−III−VI compound semiconductor, two types of metal precursors are needed. Solution A: 1 mL of indium nitrate at 0.2 M and 1 mL of citric acid at 1 M. Solution B: 0.78 mL of triethanolamine at 7.4 M mixed with 2.88 mL of sodium citrate at 0.5 M before adding an appropriate amount of silver nitrate at 0.2 M and 2.5 mL of ammonium nitrate at 0.4 M. Mix solutions A and B well for 10 min, and adjust the pH value using concentrated sulfuric acid. Then, allow this mixture to stir for 20 min before adding 6 mL of thioacetamide at 0.4 M. The detailed procedure for preparing I−III−VI compound semiconductor by using chemical bath deposition can be found in the literature.[25,26] After the precursors are prepared, place the SAM-modified substrates into the solution in an oil bath at 80 °C and then dry them in an oven at 100 °C.

Characterizations. The hydrophilic/hydrophobic properties and surface energy of SAMs can be measured using a homemade contact angle goniometer. We purchased two contact angle standards of 90° and 39.6° from Pentad Scientific Corp. The average standard contact angles of 300 measurements conducted using our contact angle goniometer were 90 ± 0.1° and 39.6 ± 0.2°. Three samples were prepared for each contact angle measurement. For the static contact angle, a sessile drop method was used. The contact angle was determined by simulating the drop shape at the vapor−liquid−solid three phase contact point. For the dynamic contact angle, we used the automated dispensing system (Rame-Hart p/n 100-22) to gradually eject/retract the contact liquid. All dynamic contact angle measurements were conducted at room temperature with the pipet tip in contact with the drop. The oxidation state on the surface was determined by an X-ray photoelectron spectroscopy (XPS, Kratos Axis Ultra DLD). The source of the X-ray is a monochromatic Al Kα ($h\nu$ = 1486.7 eV). The parameters for the XPS survey were as follows: X-ray power = 45 W, pass energy = 160 eV, step = 1000 meV, and dwell

Table 1. Water Contact Angles and AFM Results of OTS SAM Grown on Different Substrates from Various Solvents

		iso-octane		DCM		toluene		chloroform	
		I[b]	II[c]	I	II	I	II	I	II
Si	static CA[a] (H_2O, deg)	107.5	110.2	107.4	109.2	108	108.8	106.5	107.5
	dynamic contact angle hysteresis (H_2O, deg)	14	12	14	13	15	13	11	14
	roughness, Ra (nm)	0.73	0.76	0.64	0.36	0.58	0.30	0.30	0.21
	AFM cross sections max height (nm)	22.4	20	15.1	13.8	17.9	12.3	8.5	6.3
	XPS C/Si ratio	1.69	1.59	1.71	1.58	1.73	1.52	1.39	1.28
glass A	static CA	108.0	109.3	108.0	109.6	107.9	109.7	107.6	109.8
	dynamic CA hysteresis	15	17	14	20	16	16	11	11
glass B	static CA	108.2	110.3	108.3	109.1	107.9	109.4	108.2	109.1
	dynamic CA hysteresis	15	17	14	18	16	15	11	11

[a]Contact angle. [b]I: reaction temperature at 18 °C. [c]II: reaction temperature at 28 °C.

time = 100 ms. The spectrometer was configured as follows to obtain high resolution spectra with X-ray power of 60 W, pass energy of 40 eV, step of 100 meV, and dwell time of 300 ms. All spectra were calibrated at C 1s, with a binding energy of 285 eV. The surface morphology was measured using an atomic force microscope (Veeco Multimode). The tapping mode was employed. The scanning range was 2 μm. The scanning frequency was 1 Hz. X-ray diffraction patterns of $AgIn_5S_8$ crystals were recorded using an X-ray diffractometer (XRD, Shimadze XRD-6000X) with scanning rate of 4°/min. The surface morphology was observed using a field-emission scanning electron microscope (FE-SEM, Hitachi S4800–I). The energy dispersive X-ray spectroscopy (EDS) was used to conduct a qualitative analysis of the composition of the materials.

RESULTS AND DISCUSSION

Self-Assembled Monolayers on Silicon Wafers and Glass Substrates. Numerous factors can affect the SAM formation, including the number of −OH groups, the cleanliness of the substrate surface, solution type, reaction temperature, water content of the solution, concentration of the surface-active molecules in solution, and the soaking sequence, etc. In terms of temperature effect, previous studies[29,37−43] have identified three regions for growing SAM. When reaction takes place at lower temperatures, SAM tends to exhibit island growth with an ordered and dense monolayer, which is called the liquid-condensed phase. When reaction takes place at high temperatures, SAM tends to exhibit uniform growth with disordered structure, which is called the liquid-expanded phase. Medium reaction temperatures are the mixed phase, where the surface morphology depends on the critical temperature (T_C). Whether the reaction temperature of SAM is higher or lower than T_C determines the ratio of the liquid-expanded phase to liquid-condensed phase. For OTS SAM, T_C is 28 ± 5 °C.[44] Our experiment results showed that when OTS SAM was grown at lower temperatures (18 °C), the static contact angles of water are 108° or below; at higher temperatures (28 °C), the static contact angles mostly exceed 108° (Table 1). When OTS SAM was grown on a glass surface, on sides A or B, the static contact angles of water ranged between 106° and 108°. The XPS data show that when OTS SAM is grown using chloroform, the C/Si ratio is the lowest. Additionally, regardless of which solution is used to grow OTS SAM, SAM grown at lower temperature has higher C/Si ratio. Therefore, with fixed number of OH^- function groups on the substrate surface, lower temperatures cause a dense monolayer, a higher C/Si ratio, and more aggregate clusters. When the reaction temperature is higher, OTS SAM tends to grow during the liquid-expanded phase. Because of fewer clusters, the C/Si ratio and the roughness decrease (Table 1). Figure 2 shows the AFM surface morphology and cross-sectional view with an average roughness of 0.21 nm. This OTS SAM was prepared on the surface of a single-crystal silicon wafer using chloroform at 28 °C. It was the smoothest SAM prepared in our laboratory and similar to the flat SAM reported in the literature.[35] Data of the dynamic contact angle hysteresis ($\Delta\theta$) show that the SAM prepared on a silicon substrate ($\Delta\theta$ = 11−14°) was smaller than that grown on a glass substrate ($\Delta\theta$ = 11−20°), which also indicates that flat and homogeneous OTS SAM can be grown on the silicon substrates.

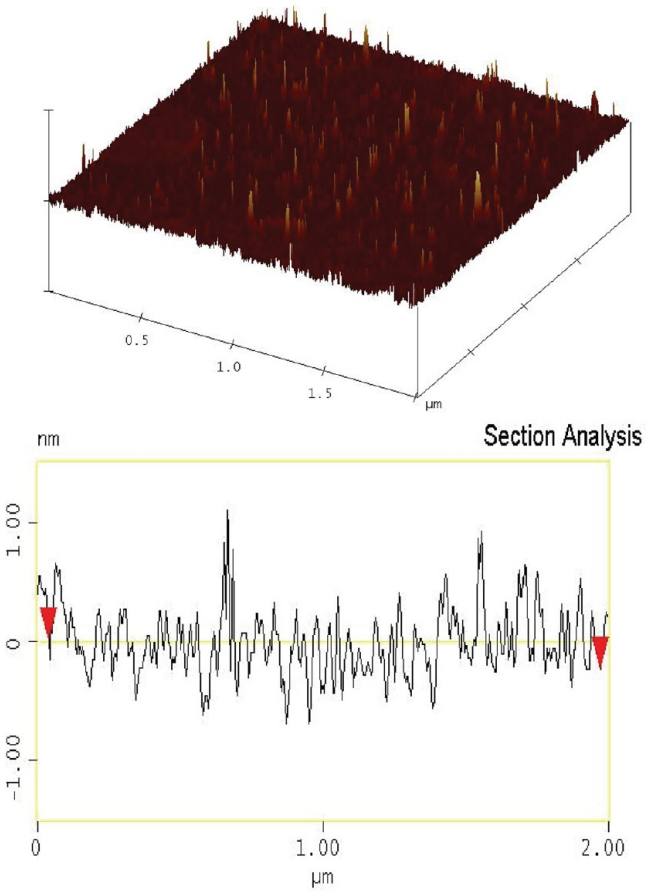

Figure 2. AFM surface morphology and a cross-sectional view of OTS SAM prepared on a silicon wafer using chloroform.

When producing mixed SAMs in one step using the OTS-MPS solution by adjusting the concentration of each ingredient, the contact angles of water were constantly 106°, regardless of

Table 2. XPS Analysis, Contact Angles, and Surface Energy with Various Concentrations of MPS and OTS mixed SAMs

	MPS−OTS (0.5−4 h)	XPS S/Si	water CA[a] (θ)	CH_2I_2 CA (θ)	γ_s (erg/cm^2)	OTS coverage
A	1:200	0.054	102.7	53.5	32.77	0.89
B	1:100	0.051	101.7	51.5	33.89	0.88
C	50:50	0.069	100.5	50.7	34.26	0.86
D	100:1	0.088	98.9	48.6	35.35	0.83
MPS		0.094	63.4	26.5	50.8	0.00
	OTS−MPS (0.5−4 h)					
E	1:200	0.053	101.1	52.6	33.13	0.87
F	1:100	0.051	101.0	52.7	33.06	0.86
G	50:50	0.050	103.9	58.9	29.50	0.91
H	100:1	0.041	107	62.1	27.83	0.96
OTS		0.0	110.2	65.7	24.9	1.00

[a]Contact angle.

the composition of the dipping solution. Feng et al.[45] stated that because of the relative reactivity, the substrate surface is first occupied by OTS molecules, and the MPS content is comparatively less. The contact angles are similar to those of pure OTS. Using this method, the time required to grow a monolayer on a substrate is not easily observed; thus, the MPS content on the substrate cannot be effectively controlled. On the basis of these studies, the two-step method to prepare the mixed SAM was employed to effectively control the MPS surface coverage. During the first stage of this two-step film formation, we soaked the substrate in the MPS solution for 30 min. The MPS molecules did not completely cover the substrate surface. During the second stage, the substrate was soaked in the OTS solution for 4 h to allow sufficient time for the OTS molecules to fill and grow in the areas without MPS, eventually forming MPS-OTS mixed SAMs. The dipping sequence can also be reversed to grow OTS−MPS mixed SAMs for comparison.

We used XPS to investigate the quantitative ratio of C, S, and Si on the substrate surface. The results show that the concentration of S on the substrate surface prepared from the two-step process is relatively higher than that from the one-step process. The S/Si ratio can be adjusted from 0.041 to 0.094 according to the preparative conditions (see Table 2). We can also use various contact solutions to calculate the surface energy and coverage ratio. Using Young's equation, that is,

$$\gamma_{sv} = \gamma_{sl} + \gamma_{lv}\cos\theta \quad (1)$$

we can estimate the surface free energy of a solid substrate (γ_{sv}), using the surface free energy of a liquid drop (γ_{lv}) and contact angle.[46] The surface free energy of water can be divided into hydrogen bonding (h) and dispersion force (d) as follows:

$$\gamma_{lv} = \gamma_l^d + \gamma_l^h \quad (2)$$

Owens and Wendt used geometric average method to simplify the problem[47] and combined the result with eq 1 to derive the following relationship for calculating the surface energy:

$$\gamma_{lv}(1 + \cos\theta) = 2(\gamma_s^d\gamma_l^d)^{1/2} + 2(\gamma_s^h\gamma_l^h)^{1/2} \quad (3)$$

When using two or more contact solutions, we can estimate the solid surface energy as the sum of the dispersion force and hydrogen bonding.

$$\gamma_{sv} = \gamma_s^d + \gamma_s^h \quad (4)$$

Using water and methylene iodide as contact liquids, we can measure the surface energy of pure MPS and pure OTS SAMs (Table 2). The surface energies of these two SAMs were similar to those reported in the literature. We can employ this simple experiment to examine the surface energy of the mixed SAM using the two-stage growing method (Table 2). Data of the contact angles show that although the surface energy decreased with increases in the OTS soaking time, the surface energy of the mixed SAM was close to the low-energy surface, indicating that OTS has a higher surface coverage ratio. The quantitative ratio of S/C in XPS also meets the trend of the measured surface energy. Additionally, data of the contact angles of mixed SAM can be used with the equation suggested by Israelachvili and Gee[48] to estimate the OTS coverage ratio. Using the two-stage growing method, within the concentration range in this study, the percentage of OTS surface was high at approximately 83−96% (see Table 2). When reducing the soaking time and the OTS solution concentration, we expected to also reduce the OTS surface coverage ratio. Thus, it is possible to adjust the ratio of each ingredient according to the specific application of mixed SAMs.

Growth of $AgIn_5S_8$ Crystals. CBD is a deposition process typically used to prepare binary metal sulfides. The S^{2-} ions are released slowly in the solution, react with the metal complex, and metal sulfides are deposited on the substrate surface. Briefly, the supersaturation of metal sulfides determines the deposition mechanism. When the degree of supersaturation is high, nanocrystallites are generated in the solution and are then attached on the substrate surface to form a film (cluster-by-cluster mechanism). When the degree of supersaturation is low, the film formation follows the ion-by-ion mechanism. However, few studies have investigated the deposition of ternary oxide or sulfide compound semiconductors using CBD. Because of its complexity, the reaction mechanism is affected by many factors, and the formation is difficult to control, increasing the difficulty of film coating. Previous study showed that induction time of each ingredient can be used to control the growth of uniform $AgIn_5S_8$ thin films on a glass substrate[26] when the substrate surface is properly engineered and the various processing parameters, such as the concentrations of each ingredient, the pH value of the solution, and the type and concentration of the complex, are adjusted. By changing the silver-to-indium ratio, we can grow all the structures appeared on the Ag_2S−In_2S_3 phase diagram on the MPS modified glass substrate.[25] The results also showed that using OTS SAM as the substrate, $AgIn_5S_8$ single crystals can be grown without any heat treatment.

In the first part of the crystal growth experiment, by carefully controlling the quality of OTS SAMs, we tried to identify the

critical factors influence the growth of $AgIn_5S_8$ crystal on the OTS-modified substrates. The nucleation and growth model suggests that a crystal cluster can be generated as a congregation of multiple seeds. The formation of large single crystals relied on the presence of limited nucleation sites.[49] Therefore, by further decreasing the seed density and controlling the supersaturation, we can grow larger and individual crystals of $AgIn_5S_8$, which are uniformly distributed on the substrate.[50,51]

We used OTS SAM, prepared in chloroform at 18 °C to modify various substrates, namely silicon wafer, glass side A, and glass side B. Ag−In−S compound semiconductors were grown by using pH 0.6 precursor solution. Figure 3 shows the SEM images of Ag−In−S semiconductors grown on various substrates. Under this parameter setting, the metal sulfide generates a filamentary structure on the glass substrates and crystal clusters on the silicon wafer. Although the morphology is similar, the surface coverage differs for the two glasses sides. The density of Ag−In−S semiconductors is higher on side A (Figure 3a) than side B (Figure 3b) of the glass. XPS data (Figure 1b) shows that the hydroxyl functional group presented on glass A is qualitatively higher than side B. Although the chemical composition varies for glass substrates, these data imply that the density of crystals is correlated with the level of −OH content. The surface of the silicon wafer shows a surface morphology of crystal clusters (Figure 3c) with a high density. The EDX analysis shows that the composition ratios of [Ag]:[In]:[S] are 1:10.8:15.8 (91.5 mol % In_2S_3) and 1:4.8:7.1 (82.8 mol % In_2S_3) for the filamentary structure and crystal grains, respectively. The ratio 1:10.8:15.8 indicates an excessive amount of [In], and 1:4.8:7.1 is close to the stoichiometric ratio of $AgIn_5S_8$. When directly observing the change in the solution color during reaction, we should see black Ag_2S in the first stage and orange In_2S_3[26] in the second stage. During the experiment, we observed that the precursor solution at a pH of 0.6 was brown in the second stage, indicating that Ag_2S may be released in the second stage. Additionally, the OTS modified glass substrate might absorb more In_2S_3 and lead to an excessive deposition of [In]. From this simple experiment, we found that in our preparation condition, the morphology of the Ag−In−S sample is not only affected by the bath of CBD, but also greatly influenced by the surface property of the substrate.

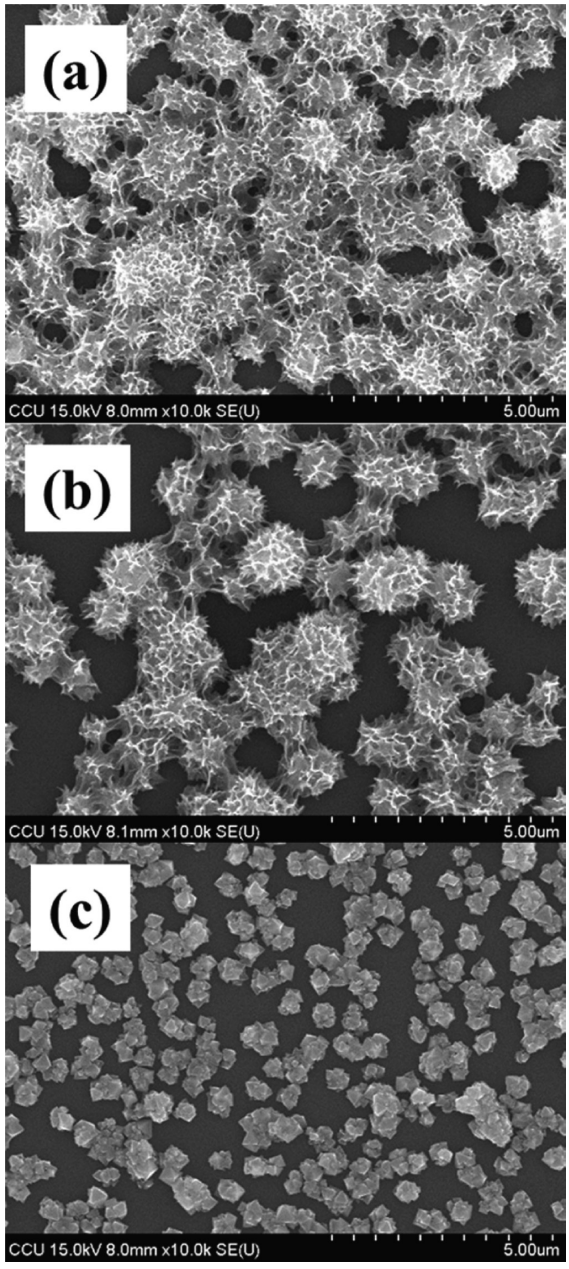

Figure 3. SEM images of Ag−In−S grown in a precursor solution with a pH of 0.6 and OTS SAM grown in chloroform at 18 °C using (a) glass side A, (b) glass side B, and (c) silicon wafer.

Figure 4a shows the XRD patterns of Ag−In−S grown on glass A, glass B, and silicon wafer, as well as the standard peak positions of $AgIn_5S_8$ powdered sample (JCPDS 25-1329). All the samples have the spinel crystal structure. The peak intensities of the samples grown on the silicon substrate are much higher than those of the other samples, indicating a more crystalline nature. Note also that the peak positions of the samples grown on glass substrates, both side A and side B, shifted to higher angles, indicating a smaller lattice constant. The phase diagram of Ag_2S−In_2S_3 shows that the single phase solid solution appears between 83 and 96 mol % of In_2S_3.[52] In this single phase region, the lattice constant will decrease continuously from 1.08265 ($AgIn_5S_8$) to 1.0774 nm (β-In_2S_3). From the EDX data, the compositions of all these three samples reside in this single-phase region. The samples on glass substrates that have higher level of indium content also display higher diffraction angles, which agree with the XRD analysis (Figure 4b).

Hsu et al.[53] reported that the attraction between the functional group in the organic monolayer and metal ions in the solution determines the morphologies of the inorganic thin films (2D or 3D) grown on the substrate, depending on the degree of the metal ion absorption. Because the growing mechanism of Ag−In−S semiconductors is a two-stage reaction,[25,26] the growth rate of Ag_2S on the substrate surface in the first stage is critical to the final composition of the $AgIn_5S_8$ crystals. Ma et al. also[54] reported that the nucleation and growth in the solution correlates with the degree of supersaturation of the precursor. When the solution is oversaturated, it produces a seed crystal. After the formation of the seed crystal, the supersaturation decreases. The solution only produces another seed crystal when the ion concentration again exceeds the supersaturation. With the fluctuating supersaturation in the solution, the new seed crystal attaches to the existing seed crystal, continues to grow, and eventually forms clusters. If the Ag_2S is generated during the second stage,

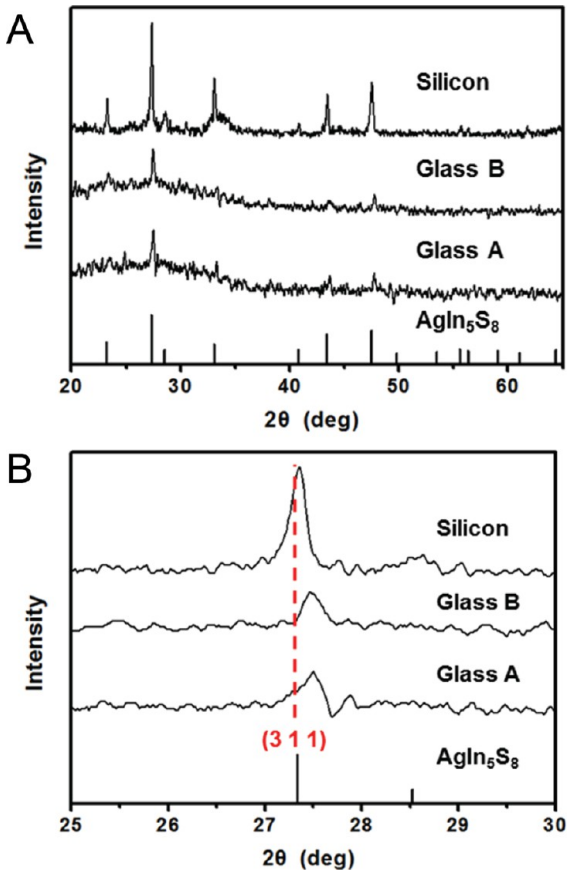

Figure 4. X-ray diffraction patterns of (a) Ag−In−S crystals grown on silicon wafer, glass side A, and glass side B and (b) an enlargement of XRD patterns between 25 and 30°.

it may directly react with In_2S_3 and produce Ag−In−S compounds in the solution, reducing the amount of In_2S_3 that attaches to the substrate in the solution. If the new Ag_2S attaches to the existing Ag_2S on the substrate, it may generate clusters. Therefore, the filamentary structure in the SEM images may result from the new In_2S_3 that attaches to the existing clusters. Although the nucleation mechanism for growing $AgIn_5S_8$ grains on a substrate is complicated and affected by numerous parameters, changing the parameters of precursor solutions is a feasible method for preventing $AgIn_5S_8$ crystals from clustering together. In the following experiment, we used the OTS SAM-modified silicon substrate and altered the precursor concentration in order to obtain larger crystals. We also explored the key surface properties that influence the growth of single crystal $AgIn_5S_8$.

When reducing the pH value of the precursor solution from approximately 0.6−0.1 using sulfuric acid, the largest change is that the transition period between these two stages becomes significant. After the first reaction stage, the solution becomes clear with a black Ag_2S precipitates at the bottom of the bottle when stirring is turned off. During the second reaction stage, the precursor solution becomes orange rather than brown. This may be because In^{3+} ions are released at a higher rate and react rapidly with S^{2-} ions in the solution when the pH value decreases. Using SEM (Figure 5), we found that the $AgIn_5S_8$ clusters grown on the substrate decline significantly and the surface density decreases. Meanwhile, the $AgIn_5S_8$ crystal size increases significantly, compared to Figure 3c. The maximum diameter of a single grain is approximately 1 μm and crystal

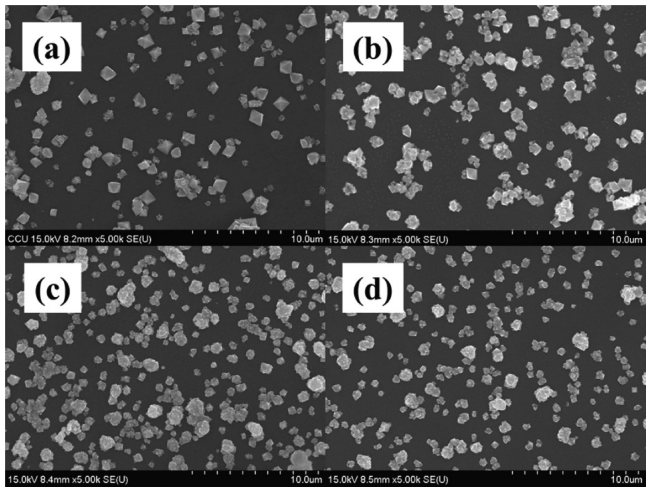

Figure 5. SEM micrographs of Ag−In−S crystals grown on SAM-modified single-crystal silicon wafer substrates. SAM-growing solutions, that is, (a) chloroform, (b) toluene, (c) DCM, and (d) iso-octane.

density of approximately 0.038/μm^2, as shown in Figure 6a. The powder XRD result shows that the crystal has $AgIn_5S_8$ spinel structure (Figure 6b). Previous studies have shown that when the nucleation sites are concentrated,[49,54,55] the crystals tend to cluster together. Only a single nucleation site results in the growth of an individual crystal. Because Ag−In−S has two reaction stages, the ion-by-ion growing mechanism is not

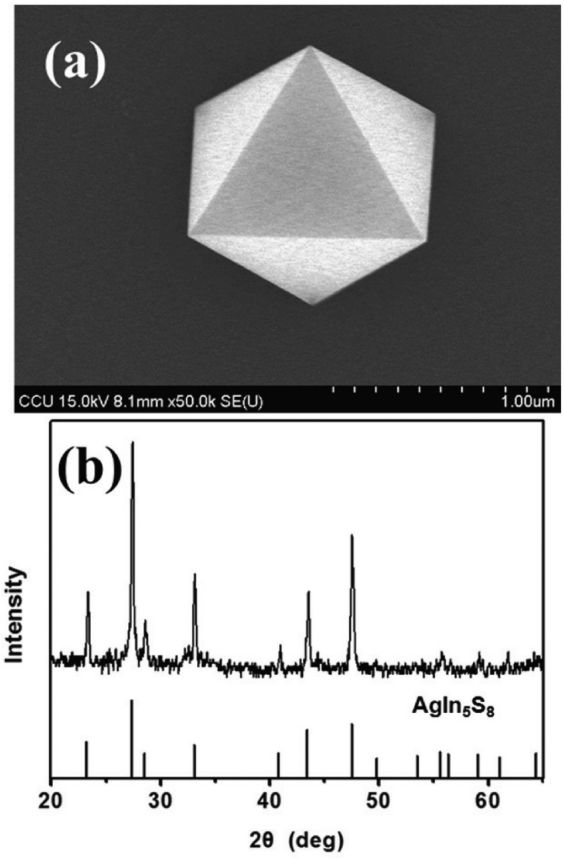

Figure 6. (a) SEM image of a $AgIn_5S_8$ crystal with a bipyramid structure. (b) XRD pattern of $AgIn_5S_8$ crystal.

applicable. By reducing the pH value of the precursor solution, the concentration of silver and indium ions can be suppressed to reduce the nucleation sites on the substrate. The surface property also plays a critical role, which will be discussed in the following paragraph. Comparing SEM images of the same area, we found that the total size of $AgIn_5S_8$ clustered together is similar to that of distributed single $AgIn_5S_8$ grains. Therefore, the total amount of In_2S_3 absorbed on the substrates must be constant. By reducing the nucleation sites, $AgIn_5S_8$ can grow into a larger crystal. Wang et al.[56] used a similar method to grow bismuth sulfide with a three-dimensional structure, suppressing the number of nucleation sites for sulfide ions by reducing the pH value of the solution. The quantity of bismuth sulfide increases as the duration of the solution reaction increases.

In our previous studies,[25,26] we have demonstrated that substrate surface with −SH functional group can increase the nucleation density of Ag_2S, due to chemical affinity between −SH and metal/metal sulfide. We also proposed a two-step mechanism for Ag−In−S deposition because of the solution chemistry in the precursor solution. To further understand the physical origin of $AgIn_5S_8$ crystal growth on $-CH_3$ terminated surface, OTS SAMs prepared using various solutions were scrutinized. Again, Figure 5 shows $AgIn_5S_8$ on OTS SAM grown on silicon wafer substrates using four different solvents prepared at 28 °C. After the OTS SAM was prepared, XPS was employed to determine the content of −OH groups on the surface quantitatively (Table 3). The OTS grown in the chloroform had the least −OH groups, the roughness of the SAM was 0.21 nm (Table 1), which was the smoothest. The −OH groups of SAM grown in the iso-octane solution were 1.73 times higher than those grown in the chloroform solution. The roughness of the SAM was 0.76 nm, and the SAM surface contained OTS aggregates. The $AgIn_5S_8$ coverage of SAM prepared in the chloroform (Figure 5a) was less than that prepared in the iso-octane (Figure 5d). The roughness and level of −OH functional groups might affect the crystal density of $AgIn_5S_8$. If we focus on the OTS SAM prepared in toluene, roughness, and the percentage of −OH groups was nearly identical to those prepared in the chloroform solution. The density of $AgIn_5S_8$ crystals grown on the toluene substrate surface (Figure 5b) was slightly higher than that prepared in the chloroform. The roughness of OTS SAM prepared using DCM (0.36 nm) was slightly higher than that prepared using chloroform and similar to that prepared using toluene. However, this OTS has more −OH functional groups (2.4% v.s. 1.4% using toluene and 1.5% using chloroform) and has a higher $AgIn_5S_8$ crystal density than the SAMs prepared by toluene and chloroform. Note that the surface of the SAM prepared by iso-octane was rougher than that prepared by DCM; however, they had a similar number of −OH functional groups and $AgIn_5S_8$ crystal density. Although we did not conduct precise quantitative analysis of the −OH content on the SAM-modified substrate surface, the preceding arguments indicate that the −OH group content has a greater influence on the $AgIn_5S_8$ coverage than the surface morphology of SAM.

Table 3. XPS O_{1s} High-Resolution Analysis of OTS SAMs Prepared in Various Solvents

	iso-octane	DCM	toluene	chloroform
O−H (%)	2.6	2.4	1.4	1.5
O−Si−O	93.9	94.7	96.4	96.2
C−O	3.5	2.9	2.2	2.3

When an OTS SAM immersed in a solution with a pH less than 4, the unreacted OH groups on the OTS modified substrate surface result in positive charge on the surface.[57] We presume that during the first reaction stage, the SAM surface absorbs negative sulfide ions and then reacts with silver ions to form Ag_2S. In the second reaction stage, In_2S_3 deposits on top of Ag_2S to generate Ag−In−S compound semiconductor. Therefore, if the substrate surface contains large amounts of Ag_2S, the $AgIn_5S_8$ crystals are smaller and clustered together. If the Ag_2S nucleation on the SAM surface decreases with scattered distribution, In_2S_3 then attaches to and reacts with Ag_2S, forming distributed single $AgIn_5S_8$ crystals on the OTS modified silicon wafer substrate. On the basis of the aforementioned observations and our previous reports,[25,26] we postulate a deposition mechanism within the given experimental systems, as shown in Figure 7. The deposition is divided into two pathways. First, when the active −SH groups are presented on the surface, the coordination between silver ions in the solution and thiol will take place. The coordinates might react with S^{2-} released from TAA in precursor solution. The Ag_2S seed layer was then generated. On the other hand, when $-CH_3$ groups are presented on the surface, this functional group is inert toward Ag^+ ions and thus prevents nucleation on the surface. In this case, −OH groups are responsible for the nucleation of Ag_2S seeds. At the second stage of the Ag−In−S crystal growth process, In_2S_3 is then deposited on top of the Ag_2S seed layer, according to the induction time experiment. This layered structure is then merged to a single phase silver indium sulfide compound, typically $AgIn_5S_8$ in this study, due to interdiffusion of atoms at an elevated temperature (80 °C in chemical bath). By suitable control of the surface properties of the substrate and solution chemistry in the precursor simultaneously, Ag−In−S crystals with a desired composition can be custom-made. Comparing the reactivity between −OH and −SH terminated substrate

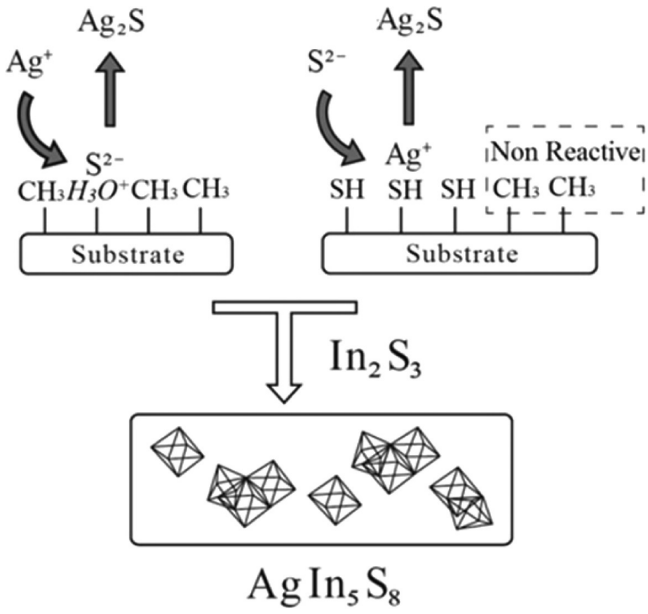

Figure 7. Growth mechanism of $AgIn_5S_8$ crystals on OTS and MPS SAM.

surfaces, we have demonstrated that thiol groups are more active than hydroxyl groups, judged by nucleation density.[25] Therefore, we believe that, for OTS−MPS mixed SAMs, surface coverage of MPS controls the $AgIn_5S_8$ crystal growth process, which will be demonstrated in the following section. On the other hand, −OH functional groups are responsible for nucleation and growth of $AgIn_5S_8$ crystals on the OTS SAM.

Photoelectrochemical Performance of $AgIn_5S_8$ Crystals. One of the applications of $AgIn_5S_8$ crystals is hydrogen production from water splitting. In this study, photoelectrochemical system was utilized to demonstrate the feasibility of low-temperature grown energy materials without any post heat treatment process. Our previous study showed that crystalline $AgIn_5S_8$ films can be deposited on the pure MPS-modified glass substrate after 400 °C annealing.[25] Therefore, mixed OTS−MPS SAMs were used as the substrates, in order to obtain crystalline $AgIn_5S_8$ without any heat treatment. For growing Ag−In−S thin films on mixed SAMs, the results show that the growth of $AgIn_5S_8$ crystals still follows the two-stage growth mechanism we proposed.[26] Ag_2S was first deposited on the substrate surface, followed by the growth of In_2S_3 on top of the Ag_2S surface. After a period of reaction time, $AgIn_5S_8$ crystals were obtained. MPS provides nucleation sites for Ag_2S, and the nucleation density determines the final structure of the films. The D, F, G, and H samples, listed in Table 2 were used as substrates to grow Ag−In−S thin films. These four samples were selected because their OTS surface coverage ratios varied greater under our experimental conditions (D 83% OTS, F 86%, G 91%, and H 96%). With decreases in the MPS surface coverage ratio (D → H), the density of Ag−In−S decreases and the semiconductor grain size increases, as shown in Figure 8. These SEM images show the

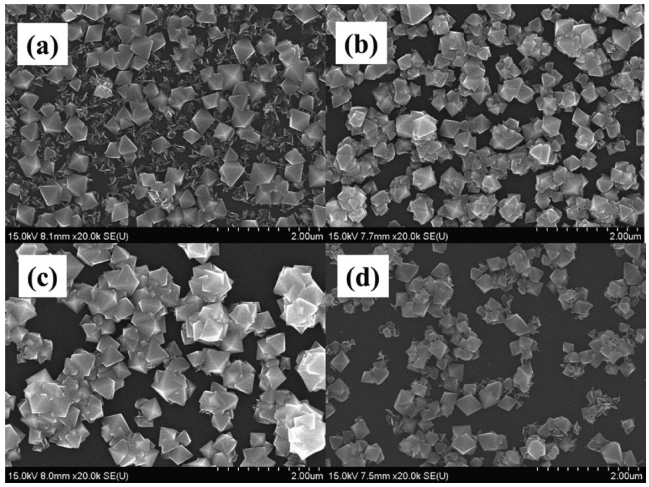

Figure 8. Ag−In−S crystals grown using OTS-MPS-mixed SAM with various surface energies: (a) sample D, (b) sample F, (c) sample G, and (d) sample H. Sample numbers are listed in Table 2.

as-prepared samples, which indicate that without heat treatment, growing Ag−In−S crystals on the substrate surface is feasible. The density of Ag−In−S satisfied the trend mentioned previously. However, the size of the crystals is significantly affected by the solution chemistry. In fact, controlling the nucleation density is relatively easier. X-ray diffraction measurements were carried out for samples D (Figure 8a) and G (Figure 8c). We found that the crystals grown on the mixed SAM-modified substrates have an $AgIn_5S_8$ crystal structure (Figure 9). The qualitative analysis of XRD signals is directly compared with those of standard powder X-ray diffraction

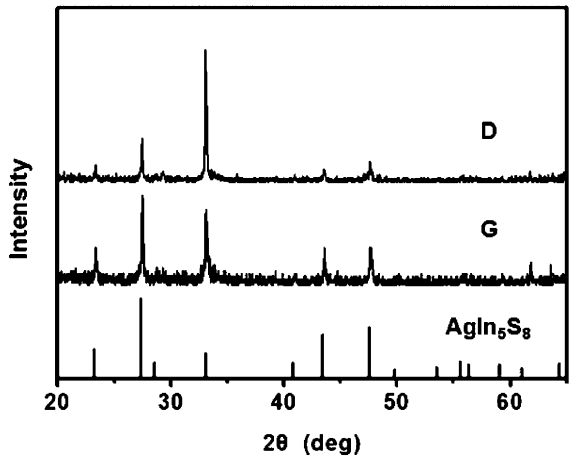

Figure 9. XRD patterns for samples D and G.

pattern (JCPDS card number 25-1329). The results show the $AgIn_5S_8$ crystals on the substrate prepared in this study have a (4 0 0) preferred orientation (2θ = 33°) (see sample D in Figure 9).

In general, photoelectrochemical hydrogen production from water is carried out using photocatalyst deposited on ITO-coated glass substrates.[23,58,59] However, SAM on silicon wafer is a well-defined system, which provides us an ideal model to study the effect the nucleation density on the growth and performance of $AgIn_5S_8$ crystals. In this study, short-chain MPS was used to tether the $AgIn_5S_8$ crystals onto the conductive substrates. Literature reported that the conductivity of the SAM is a function of thickness and dipole moment. In particular, short-chain silane molecules were used to control the work function of the ITO-coated glass substrates,[60−62] depending on the dipole moments induced by the tail functional groups. On the other hand, a highly packed SAM layer, generated from long alkylchains, blocks the electrochemical active sites on the electrode surfaces.[63−66] As a consequence, the MPS monolayer between $AgIn_5S_8$ crystals and the conductive substrate should not hinder the electron transport upon illumination. Additionally, organosilanes, both OTS and MPS, are covalently bonded to the hydroxyl group on the glass substrates and silicon wafers. SAM migration into the $AgIn_5S_8$ layer is not likely to happen. Although evidence is not provided in this study, it is believed that the SAM will remain intact.

We present here our preliminary results on the photoelectrochemical performance of relatively denser $AgIn_5S_8$ crystals (sample F); see Figure 8b. A conductive silicon wafer was used to prepare $AgIn_5S_8$ photoelectrode. A silver wire was then attached to the sample with silver paste. The back and sidewalls were covered with epoxy resin. The area of the sample was kept at 1 cm^2. The photoelectrochemical properties were recorded with a three-electrode setup. A 300 W Xe lamp with intensity of 100 mW/cm^2 was used as the light source for the photoactivity measurement. Figure 10 shows the photocurrent density of this sample under bias 0 V vs SCE. The steady photocurrent density is approximately 0.7 $\mu A/cm^2$. The inset shows the linear sweep voltammetry of sample F with applied potential from −1.5 to 1.0 V vs SCE, by using chopping method. The large dark current, starting around 0.0 V vs SCE implies a huge electron−hole recombination. It can be seen

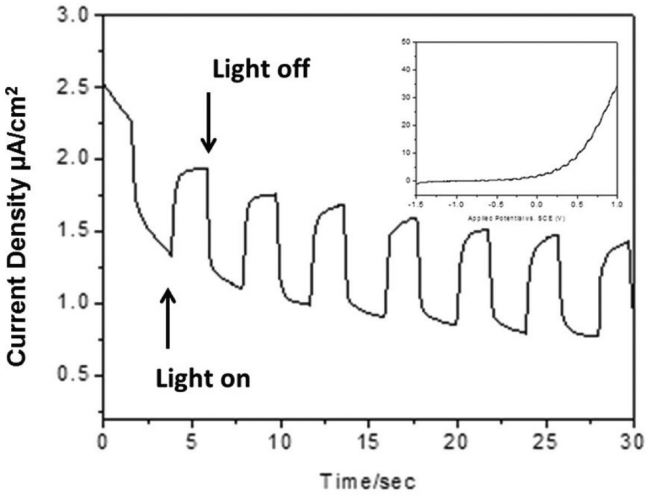

Figure 10. Photoresponse of sample F under 0 V vs SCE.

from Figure 8b that the silicon substrate exposes to the electrolyte during photoactivity experiment. The $AgIn_5S_8$ crystals did not cover the substrates completely. The void areas might be the electron−hole recombination centers that contribute to the high dark current. Indeed, the photoresponse of $AgIn_5S_8$ films prepared using chemical bath deposition is much higher than the crystals prepared in this study.[23,24,27] In fact, many factors may influence the photoelectrochemical response, such as the crystal structure, the energy alignment, grain boundary, carrier transport behavior, electron−hole recombination probability, etc.[67] This study demonstrated that a low-temperature process can be used to generate $AgIn_5S_8$ crystals for energy applications. However, the condition is not optimized. For example, the optimal ratio of MPS/OTS that generates the best contact between $AgIn_5S_8$ crystals and substrates is not determined. This optimal condition might be able to decrease the electro-hole recombination centers. This proof-of-concept experiment demonstrates that the sample prepared from our low-temperature process shows positive photoactivity, which can be used for future applications, such as solar cells and hydrogen generation from water splitting.

CONCLUSION

In this study, we reexamined MPS, OTS, and MPS−OTS-mixed SAMs. We designed a process to maneuver the surface property of the substrate. The surface free energy of the substrate was systematically controlled after the treatment. By adjusting the solution chemistry, we can easily tune the nucleation on the substrate surface, enabling us to obtain $AgIn_5S_8$ crystals with bipyramid structure without any post thermal treatment. The quality of SAM is extremely sensitive to the solution, temperature, and substrate surface properties. The morphology of SAM on the substrate surface slightly changes the physical and chemical properties, such as wettability, surface energy, and functional groups. CBD is easily affected by reaction parameters, as well as the substrate properties, and using it to produce a large uniform thin film is difficult. However, this research has demonstrated that with appropriate control of the solution chemistry and surface properties, the nucleation density (crystal density) on the surface can be easily tuned. The photoelectrochemical property of the as-prepared sample was also given. This fabrication process for composite semiconductor crystals provides a new direction for chemical deposition.

AUTHOR INFORMATION

Corresponding Author

*E-mail: taichoulee@ncu.edu.tw.

Notes

The authors declare no competing financial interest.

ACKNOWLEDGMENTS

We appreciate the sponsorship for this project received from the National Science Council (NSC 98-2221-E-194-032 and NSC 99-2221-E-008-110) and the assistance from the Instruments Center at National Chung Cheng University in conducting instrumental analysis (SEM, XPS, and AFM).

REFERENCES

(1) Lodhi, M. A. K. *Int. J. Hydrogen Energy* **2004**, *29*, 1099−1113.
(2) New Energy Policy of Taiwan. http://web3.moeaboe.gov.tw/ECW/english/content/Content.aspx?menu_id=969 (accessed June 14, 2012).
(3) Sze, S. M. Solar Cells. *Physics of Semiconductor Devices*, 2 ed.; Jonh Wiley & Sons: New York, 1981; pp 790−838.
(4) Contreras, M. A.; Romero, M. J.; To, B.; Hasoon, F.; Noufi, R.; Ward, S.; Ramanathan, K. *Thin Solid Films* **2002**, *403*−*404*, 204−211.
(5) Pudov, A. O.; Sites, J. R.; Contreras, M. A.; Nakada, T.; Schock, H.-W. *Thin Solid Films* **2005**, *480*−*481*, 273−278.
(6) Bak, T.; Nowotny, J.; Rekas, M.; Sorrell, C. C. *Int. J. Hydrogen Energy* **2002**, *27*, 991−1022.
(7) Ashokkumar, M. *Int. J. Hydrogen Energy* **1998**, *23*, 427−438.
(8) Eisenberg, R.; Nocera, D. G. *Inorg. Chem.* **2005**, *44*, 6799−6801.
(9) Kudo, A. *Int. J. Hydrogen Energy* **2007**, *32*, 2673−2678.
(10) Grätzel, M. *Nature* **2001**, *414*, 338−344.
(11) Makhova, L.; Szargan, R.; Konovalov, I. *Thin Solid Films* **2005**, *472*, 157−163.
(12) Muller, K.; Milko, S.; Schmeiber, D. *Thin Solid Films* **2003**, *431*−*432*, 312−316.
(13) Deivaraj, T. C.; Park, J.-H.; Afzaal, M.; O'Brien, P.; Vittal, J. *Chem. Mater.* **2003**, *15*, 2383−2391.
(14) Albor Aguilera, M. L.; Ortega-Lopez, M.; Sanchez Resendiz, V. M.; Aguilar Hernandez, J.; Gonzalez Trujillo, M. A. *Mater. Sci. Eng., B* **2003**, *102*, 380−384.
(15) Bereznev, S.; Konovalov, I.; Opik, A.; Kois, J. *Synth. Met.* **2005**, *152*, 81.
(16) Podder, J.; Miyawaki, T.; Ichimura, M. *J. Cryst. Growth* **2005**, *275*, e937−e942.
(17) Pathan, H. M.; Lokhande, C. D. *Appl. Surf. Sci.* **2005**, *245*, 328−334.
(18) Gao, Y.; Koumoto, K. *Cryst. Growth Des.* **2005**, *5*, 1983−2017.
(19) Dona, J. M.; Herrero, J. *J. Electrochem. Soc.* **1994**, *141*, 205−210.
(20) Froment, M.; Lincot, D. *Electrochim. Acta* **1995**, *40*, 1293−1303.
(21) O'Brien, P.; McAleese, J. *J. Mater. Chem.* **1998**, *8*, 2309−2314.
(22) Yamaguchi, K.; Yoshida, T.; Lincot, D.; Minoura, H. *J. Phys. Chem. B* **2003**, *107*, 387−397.
(23) Chang, W.-S.; Wu, C.-C.; Jeng, M.-S.; Cheng, K.-W.; Huang, C.-M.; Lee, T.-C. *Mater. Chem. Phys.* **2010**, *120*, 307−312.
(24) Cheng, K.-W.; Huang, C.-M.; Pan, G.-T.; Chang, W.-S.; Lee, T.-C.; Yang, T. C. K. *J. Photochem. Photobiol. A* **2007**, *190*, 77−87.
(25) Lin, L.-H.; Wu, C.-C.; Lai, C.-H.; Lee, T.-C. *Chem. Mater.* **2008**, *20*, 4475−4483.
(26) Lin, L.-H.; Wu, C.-C.; Lee, T.-C. *Cryst. Growth Des.* **2007**, *7*, 2725−2732.
(27) Wu, C.-C.; Cheng, K.-W.; Chang, W.-S.; Lee, T.-C. *J. Taiwan Inst. Chem. Eng.* **2009**, *40*, 180−187.
(28) Wu, C.-C.; Cho, H.-F.; Chang, W.-S.; Lee, T.-C. *Chem. Eng. Sci.* **2010**, *65*, 141−147.
(29) Ulman, A. *Chem. Rev.* **1996**, *96*, 1533−1554.

(30) Huang, L.; Nair, P. K.; Nair, M. T. S.; Zingaro, R. A.; Meyers, E. A. *Thin Solid Films* **1995**, *268*, 49−56.
(31) LiuFu, S.-C.; Chen, L.-D.; Wang, Q.; Yao, Q. *Cryst. Growth Des.* **2007**, *7*, 639−643.
(32) Masuda, Y.; Sugiyama, T.; Seo, W.-S.; Koumoto, K. *Chem. Mater.* **2003**, *15*, 2469−2476.
(33) Tarasevich, B. J.; Chusuei, C. C.; Allara, D. L. *J. Phys. Chem. B* **2003**, *107*, 10367−10377.
(34) Toworfe, G. K.; Composto, R. J.; Shapiro, I. M.; Ducheyne, P. *Biomaterials* **2006**, *27*, 631−642.
(35) Wang, Y.; Lieberman, M. *Langmuir* **2003**, *19*, 1159−1167.
(36) Modi, M. H.; Lodha, G. S.; Sawhney, K. J. S.; Nandedkar, R. V. *Appl. Opt.* **2003**, *42*, 6939−6944.
(37) Cheng, Y.-a.; Zheng, B.; Chuang, P.-h.; Hsieh, S. *Langmuir* **2010**, *26*, 8256−8261.
(38) Manifar, T.; Rezaee, A.; Sheikhzadeh, M.; Mittler, S. *Appl. Surf. Sci.* **2008**, *254*, 4611−4619.
(39) Glaser, A.; Foisner, J.; Hoffmann, H.; Friedbacher, G. *Langmuir* **2004**, *20*, 5599−5604.
(40) Glaser, A.; Foisner, J.; Friedbacher, G.; Hoffmann, H. *Anal. Bioanal. Chem.* **2004**, *379*, 653−657.
(41) Rill, C.; Glaser, A.; Foisner, J.; Hoffmann, H.; Friedbacher, G. *Langmuir* **2005**, *21*, 6289−6295.
(42) Kitaev, V.; Seo, M.; McGovern, M. E.; Huang, Y.-j.; Kumacheva, E. *Langmuir* **2001**, *17*, 4274−4281.
(43) Bush, B. G.; DelRio, F. W.; Opatkiewicz, J.; Maboudian, R.; Carraro, C. *J. Phys. Chem. A* **2007**, *111*, 12339−12343.
(44) Parikh, A. N.; Allara, D. L.; Azouz, I. B.; Rondelez, F. *J. Phys. Chem.* **1994**, *98*, 7577−7590.
(45) Feng, J.; Xu, G. H.; An, Y.; Zeng, X. *Colloids Surf. A* **2008**, *316*, 194−201.
(46) Fowkes, F. M. *J. Phys. Chem.* **1963**, *67*, 2538−2541.
(47) Owens, D. K.; Wendt, R. C. *J. Appl. Polym. Sci.* **1969**, *13*, 1741−1747.
(48) Israelachvili, J. N.; Gee, M. L. *Langmuir* **1989**, *5*, 288−289.
(49) Wucher, B.; Yue, W.; Kulak, A. N.; Meldrum, F. C. *Chem. Mater.* **2007**, *19*, 1111.
(50) Niu, W.; Zheng, S.; Wang, D.; Liu, X.; Li, H.; Xu, G. *J. Am. Chem. Soc.* **2009**, *131*, 697−703.
(51) Niu, W.; Zhang, L.; Xu, G. *ACS Nano* **2010**, *4*, 1987.
(52) Sachanyuk, V. P.; Gorgut, G. P.; Atuchin, V. V.; Olekseyuk, I. D.; Parasyuk, O. V. *J. Alloy. Compd.* **2008**, *452*, 348−358.
(53) Hsu, J. W. P.; Clift, W. M.; Brewer, L. N. *Langmuir* **2008**, *24*, 5375−5381.
(54) Ma, Y.-Y.; Jiang, Z.-Y.; Kuang, Q.; Zhang, S.-H.; Zheng, L.-S. *J. Phys. Chem. C* **2008**, *112*, 13405.
(55) Jose, L. E.; Jose, R.-G.; Miguel, J. Y. *J. Mater. Chem.* **2006**, *16*, 3906−3919.
(56) Liufu, S.-C.; Chen, L.-D.; Yao, Q.; Wang, C.-F. *J. Phys. Chem. B* **2006**, *110*, 24054−24061.
(57) Shyue, J.-J.; De Guire, M. R.; Nakanishi, T.; Masuda, Y.; Koumoto, K.; Sukenik, C. N. *Langmuir* **2004**, *20*, 8693−8698.
(58) Lu, Y.; Jia, J.; Yi, G. *CrystEngComm* **2012**, *14*, 3433−3440.
(59) Wang, C.-H.; Cheng, K.-W.; Tseng, C.-J. *Sol. Energy Mater. Sol. Cells* **2011**, *95*, 453−461.
(60) Jang, Y.; Cho, J. H.; Kim, D. H.; Park, Y. D.; Hwang, M.; Cho, K. *Appl. Phys. Lett.* **2007**, *90*, 132104.
(61) Kim, J. S.; Park, J. H.; Lee, J.-H.; Jo, J.; Kim, D.-Y.; Cho, K. *Appl. Phys. Lett.* **2007**, *91*, 112111.
(62) Khodabakhsh, S.; Sanderson, B. M.; Nelson, J.; Jones, T. S. *Adv. Funct. Mater.* **2006**, *16*, 95−100.
(63) Tremont, R. J.; Blasini, D. R.; Cabrera, C. R. *J. Electroanal. Chem.* **2003**, *556*, 147−158.
(64) Foresti, M. L.; Loglio, F.; Innocenti, M.; Bellassai, S.; Carla, F.; Lastraioli, E.; Pezzatini, G.; Bianchini, C.; Vizza, F. *Langmuir* **2009**, *26*, 1802−1806.
(65) Nagaraju, D. H.; Lakshminarayanan, V. *Langmuir* **2008**, *24*, 13855−13857.
(66) Ganesh, V.; Pal, S. K.; Kumar, S.; Lakshminarayanan, V. *J. Colloid Interface Sci.* **2006**, *296*, 195−203.
(67) Kudo, A.; Miseki, Y. *Chem. Soc. Rev.* **2009**, *38*, 253−278.